DEUTSCHES ELEKTRONEN-SYNCHROTRON
Ein Forschungszentrum der Helmholtz-Gemeinschaft

DESY 22-011
ADP-22-3/T1174
LTH 1293
arXiv:2201.10779
January 2022

Measurements of $SU(3)_f$ Symmetry Breaking in B Meson Decay Constants

S. A. De La Motte et al.

ISSN 0418-9833

NOTKESTRASSE 85 - 22607 HAMBURG

Herausgeber und Vertrieb:

Verlag Deutsches Elektronen-Synchrotron DESY

DESY Bibliothek
Notkestr. 85
22607 Hamburg
Germany

PROCEEDINGS OF SCIENCE

Measurements of $SU(3)_f$ symmetry breaking in B meson decay constants

S. A. De La Motte,[a,1,*] **S. E. Hollitt,**[a,b,1,*] **R. Horsley,**[c] **P. D. Jackson,**[a] **Y. Nakamura,**[d] **H. Perlt,**[e] **D. Pleiter,**[f] **P. E. L. Rakow,**[g] **G. Schierholz,**[h] **H. Stüben,**[i] **R. D. Young**[a] **and J. M. Zanotti**[a]

[a] *CSSM, Department of Physics, University of Adelaide, Adelaide SA 5005, Australia*

[b] *Experimentelle Physik 5, Techniche Universität Dortmund, Otto-Hahn Straße 4a, 44227 Dortmund, Germany*

[c] *School of Physics and Astronomy, University of Edinburgh, Edinburgh EH9 3FD, United Kingdom*

[d] *RIKEN Center for Computation Science, Kobe, Hyogo 650-0047, Japan*

[e] *Institut für Theoretische Physik, Universität Leipzig, 04103 Leipzig, Germany*

[f] *PDC Center for High Performance Computing, KTH Royal Institute of Technology, SE-100 44 Stockholm, Sweden*

[g] *Theoretical Physics Division, Department of Mathematical Sciences, University of Liverpool, Liverpool L69 3BX, United Kingdom*

[h] *Deutsches Elektronen-Synchrotron DESY, Notkestr. 85, 22607 Hamburg, Germany*

[i] *Universität Hamburg, Regionales Rechenzentrum, 20146 Hamburg, Germany*

E-mail: shanette.delamotte@adelaide.edu.au, sophie.hollitt@tu-dortmund.de

We present updates from QCDSF/UKQCD/CSSM on the $SU(3)_f$ breaking in B meson decay constants. The b-quarks are generated with an anisotropic clover-improved action, and are tuned to match properties of the physical B and B^* mesons. Configurations are generated with $\overline{m} = {}^1/_3(2m_l + m_s)$ kept constant to control symmetry breaking effects. Various sources of systematic uncertainty will be discussed, including those from continuum extrapolations and extrapolations to the physical point. We also present new efforts to calculate f_B and f_{B_s} using weighted averages across multiple time fitting regions. The use of an automated weighted averaging technique over multiple fitting ranges allows for timely tuning of the b-quark and reduces the impact of systematic errors from fitting range biases in calculations of f_B and f_{B_s}

The 38th International Symposium on Lattice Field Theory, LATTICE2021 26th-30th July, 2021 Zoom/Gather@Massachusetts Institute of Technology

*Speaker

1. Introduction

Experimental precision for measurements of B and B_s decays will continue to improve over the coming years, as Belle II continues collecting data and the LHCb experiment returns to operation after its upgrade period. While V_{ub} has so far been shown to have some discrepancy between determination using inclusive and exclusive semileptonic B decays [1], increased experimental precision on rare $B \to \tau\nu$ decays will soon allow competitive and independent measurements of V_{ub} using the decay constant f_B as an input.

Lattice QCD calculations of f_B using a variety of different quark actions and methods of symmetry breaking can improve the robustness of the world lattice average. Many recent contributions to the FLAG world averages [2] of f_B and f_{B_s} feature HISQ [3, 4] or Domain Wall Fermions [5], this last paper providing a new calculation to the world average of f_B/f_{B_s} relative to f_{D_s} with $N_f = 2 + 1$, which is of particular interest in these proceedings. The decay constants f_{B_s} and $f_{B_s^*}$ have also been calculated relative to f_{D_s} in a recent work using Wilson fermions [6]. All of these calculations use a fixed strange quark mass, while in this work we consider $O(a)$-improved Wilson fermions with a controlled $SU(3)_f$ breaking for the light and strange quark masses that keeps the average mass of these lighter quarks constant and fixed to the physical average mass.

2. Simulation details

2.1 SU(3) breaking and quark actions

The gauge field configurations used in this study are generated with 2+1 flavours of non-perturbatively $O(a)$ improved clover-Wilson fermions, at a variety of lattice spacings. Rather than keeping the strange quark mass m_s constant at its physical value, we follow the QCDSF process for choosing the masses of light and strange quarks [7], where the value of $\overline{m} = \frac{1}{3}(2m_l + m_s)$ is kept constant, allowing for greater control over the way in which $SU(3)$-flavour is broken. In this formalism, we expect all flavour-singlet quantities to remain approximately constant with $SU(3)_f$ —- with breaking effects at $O((\delta m)^2)$ only. This has already been demonstrated with light mesons [8].

In the specific case of B-mesons, we also expect $SU(3)$ flavour-singlet combinations of B meson properties to be approximately constant along this quark mass trajectory. We can thus use properties of the physical B flavour singlet as an appropriate target in tuning our B-mesons on the lattice. We label this B flavour-singlet meson X_B, and consider its mass $X_B^2 = \frac{1}{3}(2M_{B_l} + M_{B_s})$, or its decay constant (f_{X_B}) with an appropriate substitution. The flavour-singlet combination of light pseudoscalar masses is similarly labelled $X_\pi^2 = \frac{1}{3}(2m_K^2 + m_\pi^2)$.

We describe bottom quarks using a variant of the 'Fermilab action' or 'RHQ action' [9, 10]. This anisotropic clover-improved action has the form [11]

$$S_{lat} = a^4 \sum_{x,x'} \overline{\psi}(x') \left(m_0 + \gamma_0 D_0 + \zeta \vec{\gamma} \cdot \vec{D} - \frac{a}{2}(D^0)^2 - \frac{a}{2}\zeta(\vec{D})^2 + \sum_{\mu,\nu} \frac{ia}{4} c_P \sigma_{\mu\nu} F_{\mu\nu} \right)_{x,x'} \psi(x), \tag{1}$$

where m_0, c_P, and ζ are tuned as three free parameters. The 'best' B meson is selected by tuning the free parameters until the masses and hyperfine splitting of our calculated X_B and X_{B^*} mesons

Table 1: Table of lattice ensembles used in this work. * indicates ensembles with a different value of $\overline{m}$, further from the physical $\overline{m}$. † indicates ensembles where multiple sources per configuration are used to produce additional samples. Marked ensembles use 2 randomised sources, except for the $64^3 \times 96$ sample with 4 randomised sources used. ‡ denotes the ensemble used for the weighted averaging study explored in Section 5.1

β	a (fm)	Lattice volume	# Samples	$(\kappa_{\text{light}}, \kappa_{\text{strange}})$	m_π (MeV)	m_K (MeV)	
5.4	0.082	$32^3 \times 64$	1015	(0.11993 , 0.11993)	408	408	‡
			1004	(0.119989 , 0.119812)	366	424	
			877	(0.120048 , 0.119695)	320	440	
			1006	(0.120084 , 0.119623)	290	450	
5.5	0.074	$32^3 \times 64$	$677^\dagger$	(0.12095 , 0.12095)	403	403	
			786	(0.12104 , 0.12077)	331	435	
			1021	(0.121099 , 0.120653)	270	454	
		$32^3 \times 64$	778	(0.1209 , 0.1209)	468	468	*
			758	(0.12104 ,0.12062)	357	505	*
			$902^\dagger$	(0.121095 , 0.120512)	315	526	*
			1002	(0.121145 , 0.120413)	258	537	*
		$48^3 \times 96$	$1251^\dagger$	(0.121166 , 0.120371)	226	539	*
5.65	0.068	$48^3 \times 96$	500	(0.122005 , 0.122005)	412	412	
			500	(0.122078 ,0.121859)	355	441	
			$845^\dagger$	(0.12213 ,0.121756)	302	457	
			576	(0.122167 , 0.121682)	265	474	
		$64^3 \times 96$	$320^\dagger$	(0.122227 , 0.121563)	155	480	
5.8	0.059	$48^3 \times 96$	298	(0.12281 , 0.12281)	427	427	
			415	(0.12288 ,0.12267)	357	456	
			525	(0.12294 , 0.122551)	280	477	

match the properties of the physical X_B and X_{B^*}. The tuning method follows that in [11], where the B and B^* mesons are spin-averaged.

In practice, uncertainties on measured masses and splittings also result in uncertainty in the values of m_0, c_P, and ζ corresponding to the 'best' tuned B meson. We choose to generate multiple b-quarks per lattice ensemble in a 'tuning star' shape and interpolate to the 'best' B, rather than generating only one 'best' b-quark per ensemble. This also allows for re-interpretation of our results with newer fitting strategies, and allows us to investigate the effect of these fit strategies on the tuned b and on the final results for f_B. Where possible, we endeavour to use the same set of seven b-quarks in the tuning star for each ensemble with the same lattice spacing and volume along the line of constant $\overline{m}$.

2.2 Lattice ensembles

A variety of lattice spacings and lattice volumes are used in this work. Some details of the QCDSF gauge field ensembles are presented in Table 1.

Table 2: The calculated 'best' tuning parameters and error margins for each of the ensembles used. * denotes ensembles with a different value of $\overline{m}$, further from the physical $\overline{m}$, represented in dark blue in all Figures. † denotes the near-physical $64^3 \times 96$ ensemble which has extrapolated parameters.

β	κ_l	m_0	c_P	ζ
5.4	0.11993	3.56 ± 0.14	3.73 ± 0.36	1.59 ± 0.12
	0.119989	3.62 ± 0.13	3.88 ± 0.35	1.60 ± 0.12
	0.120048	3.58 ± 0.15	3.73 ± 0.40	1.57 ± 0.14
	0.120084	3.76 ± 0.16	4.27 ± 0.41	1.53 ± 0.14
5.5	0.12095	2.92 ± 0.13	3.86 ± 0.34	1.23 ± 0.12
	0.12104	2.82 ± 0.13	3.59 ± 0.34	1.38 ± 0.10
	0.121099	2.83 ± 0.12	3.61 ± 0.31	1.26 ± 0.11
5.5*	0.1209	2.80 ± 0.13	3.60 ± 0.34	1.30 ± 0.11
	0.12104	2.65 ± 0.11	3.19 ± 0.29	1.37 ± 0.11
	0.121095	2.86 ± 0.11	3.70 ± 0.29	1.21 ± 0.09
	0.121145	2.92 ± 0.14	3.86 ± 0.35	1.11 ± 0.14
	0.121166	2.75 ± 0.10	3.42 ± 0.25	1.34 ± 0.08
5.65	0.122005	2.67 ± 0.14	4.18 ± 0.38	1.07 ± 0.10
	0.122078	2.48 ± 0.15	3.72 ± 0.39	1.12 ± 0.11
	0.12213	2.52 ± 0.09	3.78 ± 0.24	1.16 ± 0.08
	0.122167†	2.49 ± 0.13	3.67 ± 0.34	1.25 ± 0.10
5.8	0.122227	3.18 ± 0.20	5.42 ± 0.52	0.96 ± 0.13
	0.12281	3.03 ± 0.09	5.30 ± 0.24	1.21 ± 0.07
	0.12288	3.28 ± 0.09	6.06 ± 0.27	1.14 ± 0.06
	0.12294	3.00 ± 0.08	5.25 ± 0.22	1.30 ± 0.06

The tuning parameters corresponding to the best interpolated b quark are presented in Table 2. These are calculated using our original fitting strategy, which uses the same fit window for the same correlator across each of the 7 b-quarks in the ensemble. Choosing this window is assisted by comparing the correlated χ^2/d.o.f for the fit on each B meson correlator. Limitations of this method are discussed further in Section 4.2, and the newer weighted fitting approach is discussed in detail in Section 5.

3. Decay constants

The decay constant f_B is calculated from its lattice counterpart Φ_B via the equation

$$f_{B_q} = \frac{1}{a} Z_\Phi \left[\Phi^0_{B_q} + c_A \Phi^1_{B_q} \right] \tag{2}$$

where $\Phi^0_{B_q}$ is calculated from two-point correlators for axial and pseudoscalar operators:

$$\Phi^0_{B_q} = -\frac{\sqrt{2M_B} C_{AP}}{C_{PP}}, \qquad C_{AP} = \frac{\langle \Omega | A_4 | B \rangle \ \langle B | P | \Omega \rangle}{2M_B}, \qquad C_{PP} = \frac{\langle \Omega | P | B \rangle \ \langle B | P | \Omega \rangle}{2M_B}, \tag{3}$$

and Z_Φ is calculated:

$$Z_\Phi = \rho_A^{bq} \sqrt{Z_V^{bb} Z_V^{qq}}, \tag{4}$$

where q represents the l or s quark in the calculation of f_B or f_{B_s} respectively. The perturbative constant ρ_A^{bq} is set to 1 in this work, and similarly the higher-order correction coefficient c_A in f_B is set to 0. For determining $Z_V^{bb/qq}$, we compute meson three point functions of the vector current and enforce charge conservation. In practice, Z_V^{bb} is calculated using a B_s meson.

We calculate the decay constant for each b quark in the tuning star on each ensemble, for each of 200 bootstraps. The tuning is used to linearly interpolate to the value of f_B or f_{B_s} corresponding to the best b quark. These best values are shown in Figure 1, where the error bars shown are mostly from the propagation of the uncertainties in the tuning, as most of the uncertainty from the calculation of f_{B_q} cancels when we consider the ratio f_{B_q}/f_{X_B}. Two different lines of fit are shown, one linear in $(M_\pi^2/X_\pi^2 - 1)$ and one quadratic. Both lines of best fit must pass through $(1, 1)$, and are calculated assuming that the $SU(3)_f$ breaking does not depend on the lattice spacing. The values used for comparison are calculated from FLAG world average result for f_{B_s}/f_B on $N_f = 2 + 1$ samples [2].

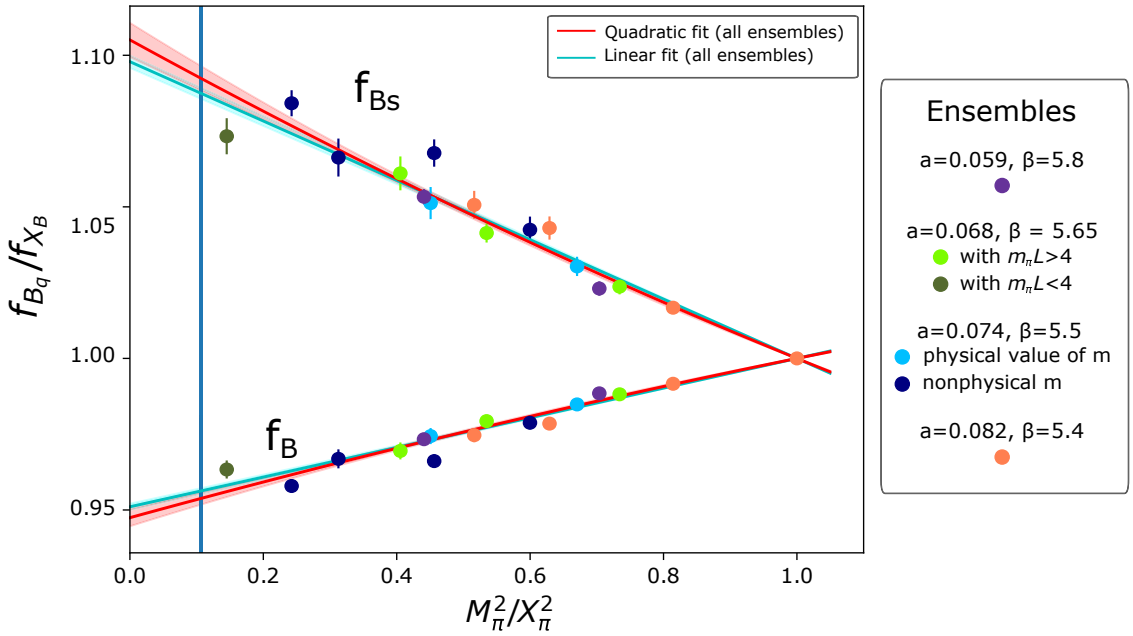

Figure 1: Fan plot of f_B/f_{B_X} and f_{B_s}/f_{B_X}, against the SU(3) breaking in the light quarks $M_\pi^2/(1/3 M_\pi^2 + 2/3 M_K^2)$.

4. Systematics and extrapolating to the physical point

4.1 The ratio f_{B_s}/f_B

In most studies, $SU(3)$ symmetry breaking in the decay constants is reported in terms of the ratio f_{B_s}/f_B. By extrapolating our calculated f_{B_s}/f_B result to the physical point, we will be able to compare our results to the FLAG averages. The ratio f_{B_s}/f_B for all ensembles is shown in Figure 2.

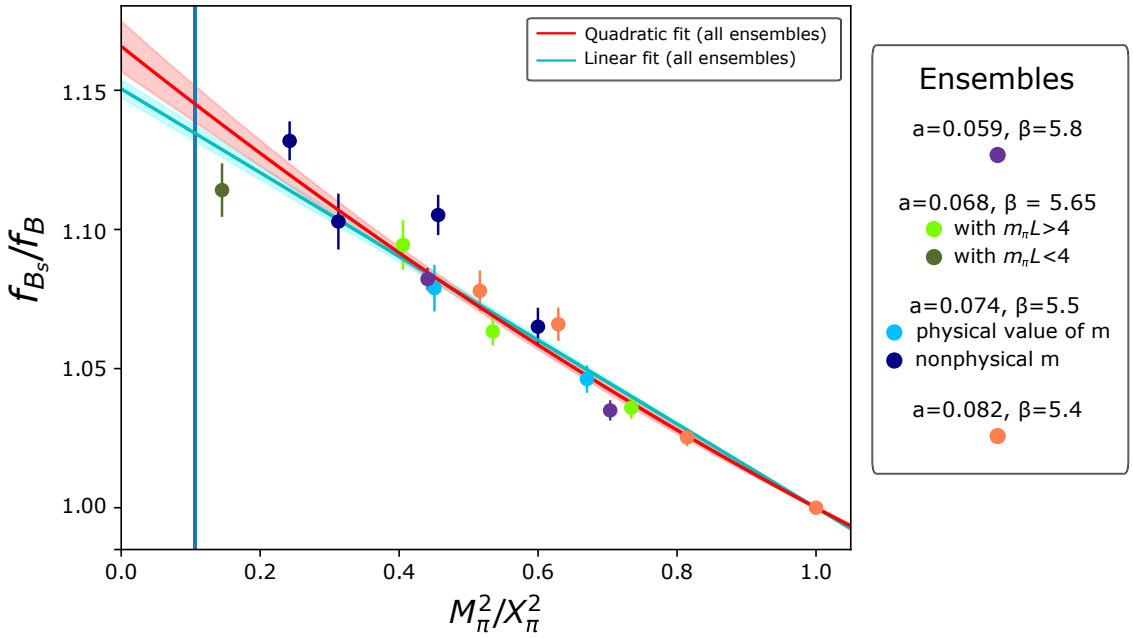

Figure 2: f_{B_s}/f_B for a variety of lattice ensembles. The linear and quadratic fits shown are for all ensembles, and are constrained to pass through the fixed point (1,1).

We observe that our ratio f_{B_s}/f_B is smaller than the $N_f = 2+1$ world average. These calculations, however, are made using an assumption that the normalisation constants Z_V^{ss} and Z_V^{ll} are approximately equal, which is only true near the $SU(3)_f$ symmetric point. From extrapolations, this separation should be 1-2 % at the physical point, which would account for some of the difference with respect to the world average. Calculation of Z_V^{ss} and Z_V^{ll} on the near-physical lattices is in progress.

In order to consider extrapolations to the physical and to the continuum limit, we make multiple fits to the decay constant ratio in order to assess the impact of lattice ensemble effects. We consider a fit of the form $f_{B_s}/f_B = H(M_\pi^2/X_\pi^2 - 1)^2 + (G_0 + G_1 a^2)(M_\pi^2/X_\pi^2 - 1) + 1$, which has quadratic and linear terms in the flavour-breaking ratio M_π^2/X_π^2. The equation is constrained to pass through the symmetric point at $(1,1)$, and we also consider the possibility of an a^2 dependence in the linear part of the expansion (coefficient G_1). Multiple fits are performed for different subsets of ensembles, including different combinations of the coefficients H, G_0, and G_1. The extrapolated results for different fit types are displayed in Figure 3, with key values also presented in Table 3. For fit functions containing the $G_1 a^2$ coefficient, the extrapolation to $M_\pi^2/X_\pi^2 = 1$ also includes the continuum extrapolation to $a^2 = 0$.

Many of the predictions for the quadratic coefficient H are consistent with zero. When the extrapolation to the physical point is performed, we see that the fits including a^2 produce a lower expected value than the other fits. From the linear and quadratic fits at individual a^2, we see somewhat of a downward trend in the extrapolated f_{B_s}/f_B results as a goes to zero. This downward trend could explain why the fits containing a^2 terms have a lower extrapolated value of f_{B_s}/f_B, but the evidence of a downward trend is not particularly strong in these ensembles and a constant relationship between f_{B_s}/f_B and a^2 is also supported by the results.

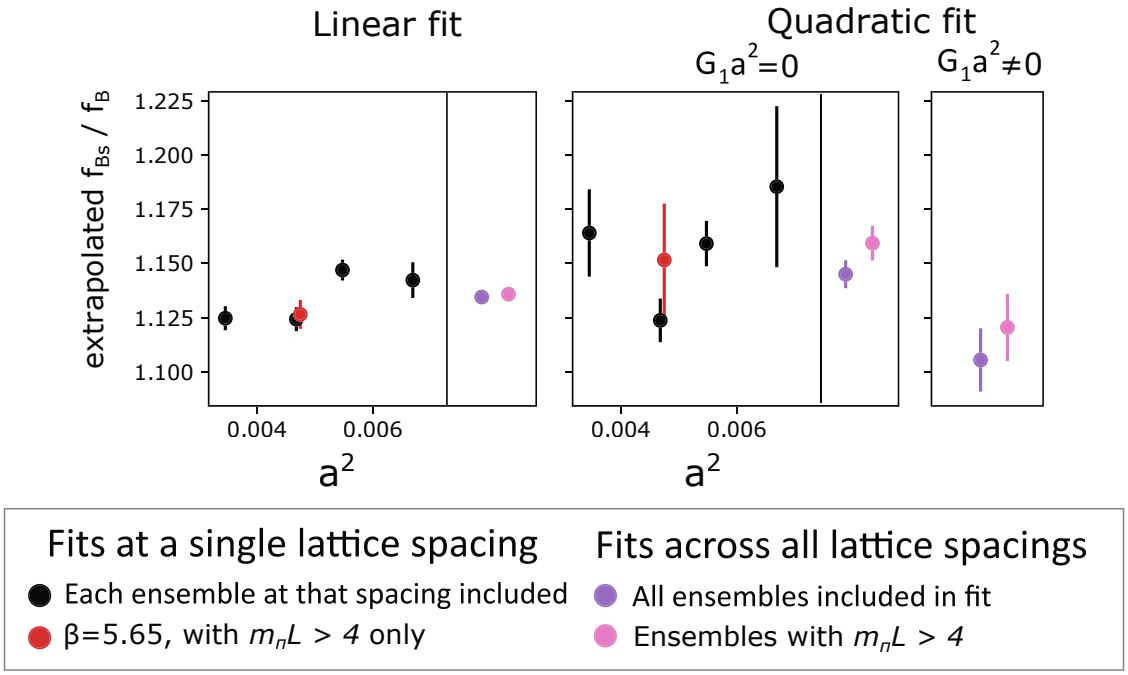

Figure 3: Extrapolated values corresponding to the physical point, for various fits to f_{B_s}/f_B.

Table 3: Extrapolated values of the f_{B_s}/f_B ratio for different fit types. The fits for $m_\pi L > 4$ include all ensembles except the near-physical pion mass $\beta = 5.65$ ensemble. * This is the combined error from FLAG

Data	Fit type	Value at physical	stat. error	χ^2/dof fit
All ensembles	Linear	1.134	0.003	1.8
	Quadratic	1.145	0.006	1.8
	Quadratic with a^2	1.105	0.015	1.3
$m_\pi L > 4$	Linear	1.136	0.003	1.8
	Quadratic	1.159	0.008	1.3
	Quadratic with a^2	1.120	0.015	0.9
FLAG value [2]		1.201	0.016*	

4.2 Results and systematic uncertainties

At this stage of the study, we choose the central value of our predictions from the $m_\pi L > 4$ ensembles, assuming no dependence on a^2. In future work with additional ensembles closer to the physical point at multiple lattice spacings, there may be more support for a dependence on a^2 and this assumption may be removed.

A summary of the estimated uncertainties for f_{B_s}/f_B is shown in Table 4. A graphical summary of the extrapolated f_{B_s}/f_B value for different scenarios is shown in Figure 4.

The systematic uncertainty of the b quark tuning method is estimated using a small study, where the fit windows used to calculate the hyperfine splitting of B and B^* are changed. This change is then propagated through to the final decay constants. We find that while the individual

Table 4: Summary of known sources of systematic error in calculation of f_{B_s}/f_B using the continuum extrapolation and quadratic extrapolation to the physical point. For a conservative estimate, errors are assumed to be uncorrelated with one another such that the total systematic is calculated in quadrature.

Source	-	+	Note
Z_V^{bb} value	0	0	Cancelled in ratio
Z_V^{ss}/Z_V^{ll}	0	0.023	2% systematic expected
Changes to b tuning	0.007	0.007	Difference between 'no b interpolation' and 'nominal'
Fitting to ensembles with light pion masses	0.015	0.015	Difference between all ensembles and $m_\pi L > 4$ for 'nominal' fits
Correlator fits used in the decay constant	0.07	0.07	Difference between 'f_B fit window' and 'nominal'
TOTAL SYSTEMATIC	**-0.071**	**+0.076**	

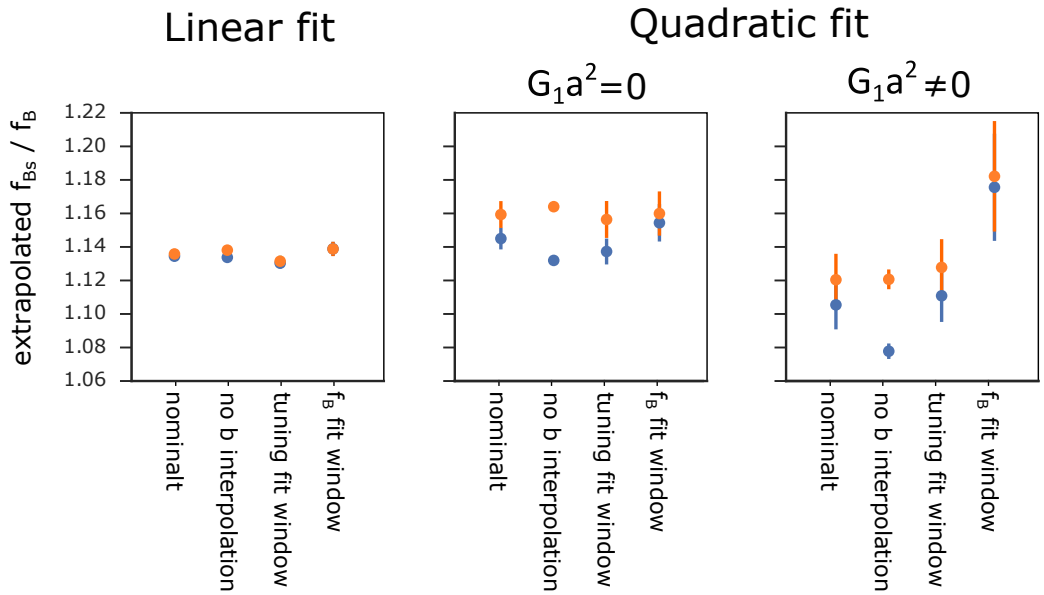

Figure 4: Extrapolated values corresponding to the physical point, for various fits to f_{B_s}/f_B. All ensembles used in fit (blue), only ensembles with $m_\pi L > 4$ used in fit (orange)

decay constants f_B and f_{B_s} are affected by these changes, the ratio f_{B_s}/f_B is minimally affected.

In contrast, the fit window used for C_{AP} has a strong effect on the results for the ratio, especially for ensembles closer to the physical point. This can also result in a failure of our assumption that the flavour singlet decay constant f_{X_B} remains approximately constant as we approach the physical point. Further investigation reveals that this discrepancy is caused by a breakdown of the earlier assumption that a similar fit window can be used for all 7 b quarks in the tuning star and for both the B and B_s cases. A systematic method is needed for choosing appropriate fit windows, that balances the need for consistency across all of the B_q mesons while also ensuring a high quality fit result for each individual correlator. In Section 5, we begin to test a weighted fit method proposed in [12, 13]

for this purpose.

We also notice that the near-physical point that is excluded from the $m_\pi L < 4$ fit has a strong effect on the final extrapolated value of f_{B_s}/f_B. This is somewhat unsurprising, as ensembles closest to the physical point are also furthest from the centre of the $SU(3)_f$ expansion, and thus will have the greatest impact on the expected quadratic component of the fit. We can see that the extrapolated values with and without the near-physical point are much more similar for the case with the changed fits for C_{AP} in the decay constant calculation.

Another interesting result is that relative to the simple quadratic fit, the physical prediction using the a^2 fit is larger in the case with where the fit windows for f_B and f_{B_s} have been adjusted, but smaller in all other cases. This change may be in part due to the larger values of f_{B_s}/f_B closer to the physical point, which are not equally distributed among all sets of ensembles.

Overall, applying these systematic uncertainties to our result from the $m_\pi L > 4$ ensembles with the quadratic fit gives

$$\frac{f_{B_s}}{f_B} = 1.159 \pm 0.015 \text{ (statistical)} \, ^{+0.076}_{-0.071} \text{ (systematic)} \tag{5}$$

at the time of this Proceedings. Adding the errors in quadrature gives $1.159^{+0.077}_{-0.073}$ which is to be compared to the FLAG value of 1.201 ± 0.016 [2].

5. Weighted averaging

The calculation of f_B and f_{B_s} requires a substantial number of distinct correlator fits, due to the tuning required for the b-quark action employed in this work. As was discussed in Section 4.2, this can lead to difficulties in controlling systematic errors from the choice of correlator fit windows. It is not practical to individually select the optimal choice of t_{min} and t_{max} for each of the $O(100)$ fits required for each ensemble. Moreover, fits chosen by eye can prove difficult when quantifying systematic error. To simplify the procedure of choosing optimal windows for many different correlators, we can calculate lattice observables as a weighted averaging over a range of t_{min} and t_{max}. We implement a weighting such that better-performing fits have the largest impact on the final average result. In this way, calculations from poorer fit windows are algorithmically suppressed without the need for additional input.

Table 5: Number of unique correlator fits required at each stage of the f_B and f_{B_s} calculation, for a given ensemble.

Correlator calculated	Number of fits per ensemble	Purpose
C_{AP}	14 (For $q = l, s$ and for each of 7 b-quarks in tuning star)	Calculate decay constant
Z_V^{qq}	2 (For $q = l, s$)	Light quark renormalisation factor of decay constant
Z_V^{bb}	7 (For each of 7 b-quarks in tuning star)	Heavy quark renormalisation factor of decay constant
$\langle B_q^*\vert V\vert\Omega\rangle$ and $\langle B_q\vert P\vert\Omega\rangle$	28 (For B_l, B_l^*, B_s, B_s^* and each of 7 b-quarks in tuning star)	Tuning to spin-averaged mass
$\frac{\langle B_q^*\vert V\vert\Omega\rangle}{\langle B_q\vert P\vert\Omega\rangle}$	14 (For $q = l, s$ and for each of 7 b-quarks in tuning star)	Tuning to mass splitting
$\langle B_q\vert P\vert\Omega\rangle$	42 (For $q = l, s$, with each of 1, 2 or 3 units of momentum and for each of 7 b-quarks in tuning star)	Tuning to kinematic mass coefficient
TOTAL (per ensemble)	107	

5.1 Implementing the weighted average technique

Our B and B_s correlators are fit over multiple choices of t_{min} and t_{max}. For each fit, a weight is determined using the correlated χ^2. Lattice quantities, such as extracted energies used in the f_B and f_{B_s} calculation, can then be calculated as an average, $\bar{x}$, over the result from each of the varied windows x_i. Each weight, w_i, is calculated and then normalised across all fits as $\frac{w_i}{\sum_j^{N_{fits}} w_j}$. The normalised weighting is combined with each window result to obtain the final result as:

$$\bar{x} = \sum_i^{N_{fits}} \frac{w_i x_i}{\sum_j^{N_{fits}} w_j}. \tag{6}$$

There are two choices of weights in the literature: a p-value based weight [12] and a Bayesian weight [13]. This study proceeds with the Bayesian weights, as it was observed that the p-value based weighting preferred short, unphysical B and B_s correlator fit windows, though this remains under investigation. The Bayesian weighting is calculated as

$$w_i = \exp(-\frac{1}{2}\chi_i^2 + N_{DOF}) \tag{7}$$

where N_{DOF} is the number of degrees of freedom. It can be seen from the form of the Bayesian weighting, that observables calculated from fits with smaller χ_i^2 and larger degrees of freedom should dominate the final weighted average result.

5.2 Simulating $B^{(*)}$ in $SU(3)_f$-symmetric ensembles

In this work, Bayesian weighted averaging is explored as a proof of concept in extracting values from B and B^* correlators. This study is performed on a single $SU(3)_f$ symmetric gauge ensemble, which was also used in decay constant calculation in Section 3. Further properties of the implemented gauge ensemble are outlined in Table 1. Treatment of the b-quark on this ensemble is identical to what is described in previous sections, thus allowing for comparison in calculations between the previous choice of best fit and what is obtained via weighted averaging. Furthermore, the analysis is restricted to a single b-quark at the centre of the tuning star, prior to interpolation. The observable to be calculated is the mass splitting $\Delta m = B^* - B$, obtained via a fit of the form $R(t) = \frac{B^*(t)}{B(t)}$ to the ratio of correlators. The fit is performed on the average of the forward and backward propagating modes in the region $t \in [0, \frac{n_t}{2}]$, being approximated by the single exponential:

$$R(t) = A\exp(-\Delta m t). \tag{8}$$

5.3 Weighted averaging method as applied to measurement of Δm of B^*-B

The mass splitting Δm_i is extracted via fits to B^*/B for each window, i. The final Δm is obtained via the weighted average procedure described in Equation 6. For this study, the weighted average is calculated from correlator fits over all possible values of t_{min} and t_{max}. The fitting windows can be parameterised so that $t \in [t_{min}, t_{max}]$ and $0 < t_{min} < \frac{n_t}{2} - 1$ and $1 < t_{max} < \frac{n_t}{2} - 1$. With $n_t = 64$ in the implemented gauge ensemble and the conditions on t described, there are 496 possible fit windows that will contribute to the final weighted average Δm. As proof of principle, there is no additional window selection criteria even for windows well into the noisy region of the correlator.

It is assumed for now that additional window selection criteria for 'good' windows is currently not necessary, as the weighting will be small enough that the effect of these wayward measurements will be minimal. Quantifying this is a topic of further study.

5.4 Results

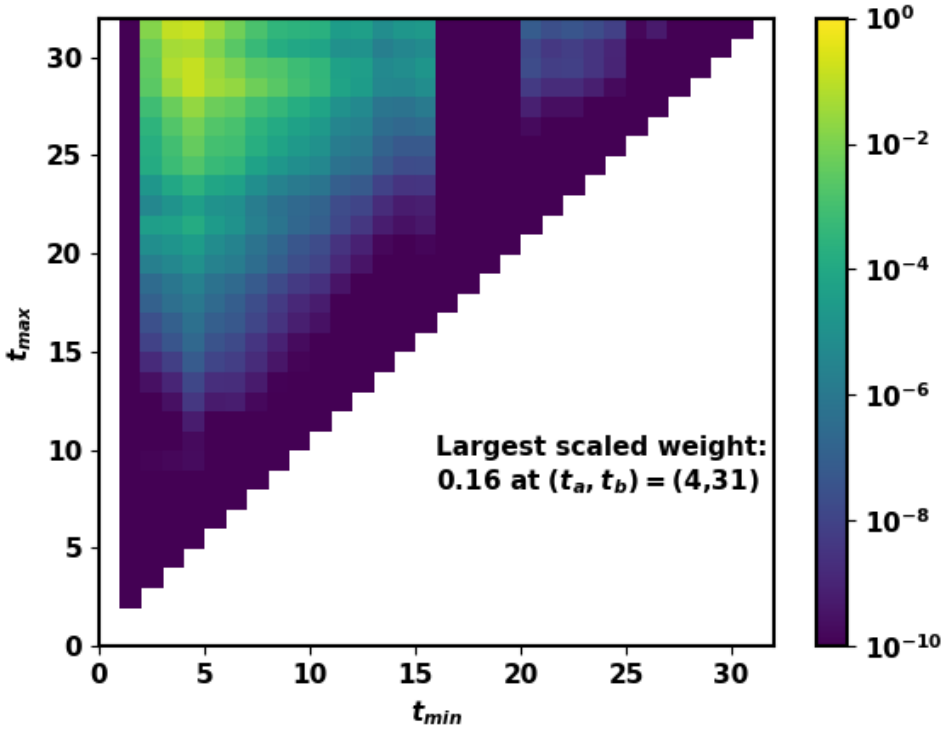

Figure 5: Heatmap of Bayesian weights against t_{min} and t_{max}.

The weights evaluated for the 496 choices of t_{min} and t_{max} are plotted in Figure 5. The larger weights generally arise from longer fit windows, even when they extend well into the noisy region. With the largest weights, the Δm_i calculated on longer plateau lengths dominate the weighted average result. This demonstrates a susceptibility of the Bayesian implementation of weighted averaging: that as windows increase T into the noisy region, the χ_i does not increase at the same rate, meaning that w_i remains large with a preference for these more difficult regions. To avoid this, future implementations could limit which t_{max} fits were allowed into the weighted average. The fit window with the highest weight is $t \in [4, 31]$, one such long fit.

The weighted average over all 496 windows of the $B^* - B$ mass splitting was found to be $a\Delta m = 0.140 \pm 0.070(\text{sys}) \pm 0.020(\text{stat})$. This value is consistent with the traditional single-window output parameters in Figure 7a (analyst choice of window) and Figure 7b (example of poorer choice).

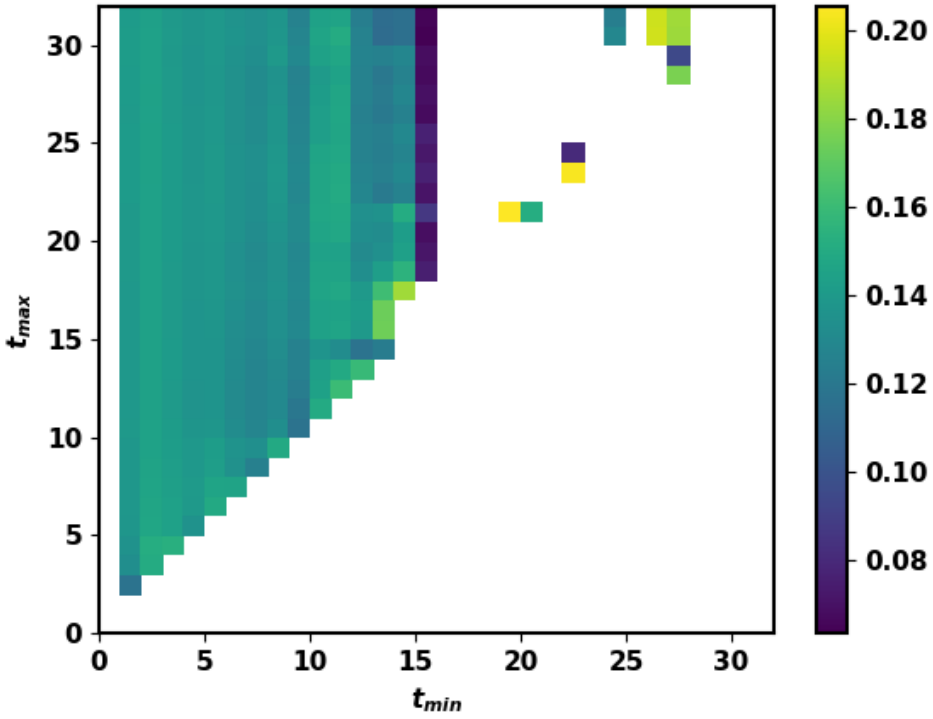

Figure 6: Heatmap of Δm_i against t_{min} and t_{max}, for Δm_i within $\pm(\sigma_{sys} + \sigma_{err})$

6. Conclusion

We present a result $f_{B_s}/f_B = 1.159 \pm 0.015\,\text{(statistical)}\,^{+0.076}_{-0.071}\,\text{(systematic)}$ using QCDSF/UKQCD ensembles with controlled $SU(3)_f$ breaking. Further work is in progress to reduce the systematic uncertainty in this measurement. In particular, we explore a weighted fitting strategy as a method to reduce the uncertainty from fit window choice in calculated f_{B_s}/f_B values for ensembles close to the physical point, as the optimal window limits vary with the parameters of the RHQ action.

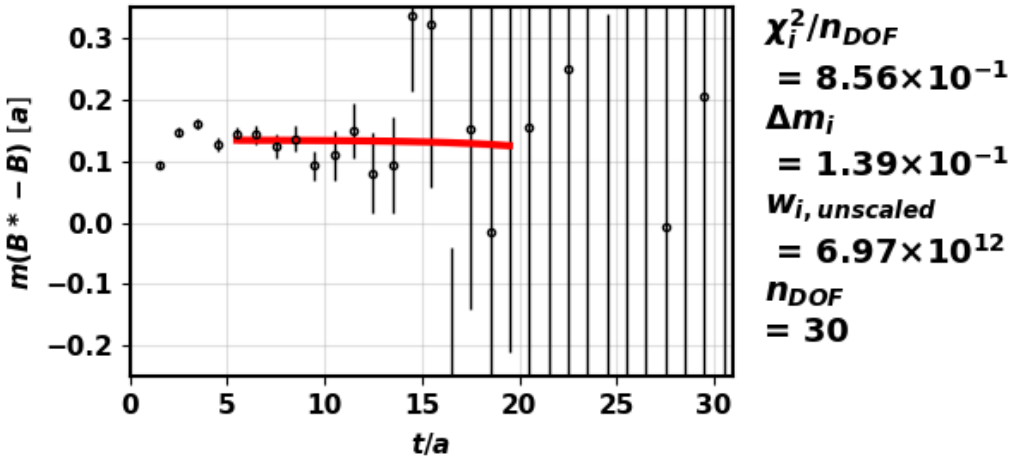

(a) Moderate weighting, example analyst window choice: $t \in [5, 20]$

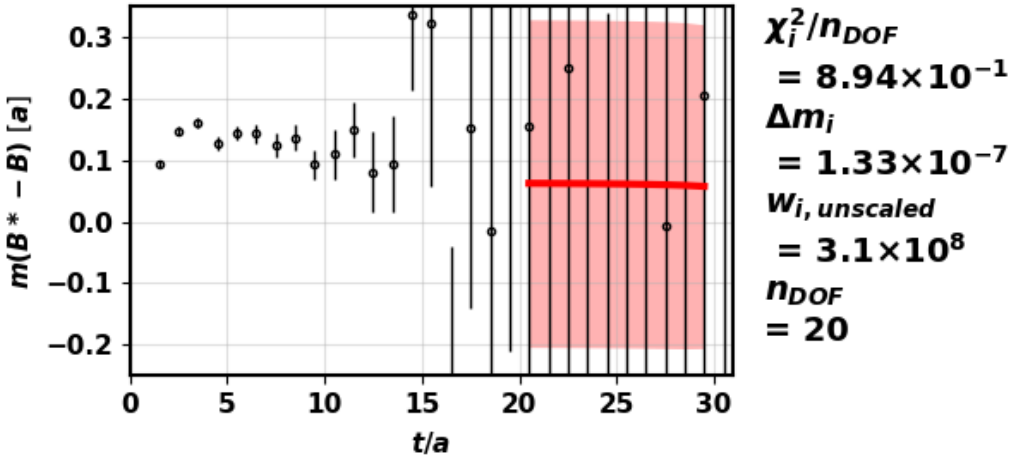

(b) Low weighting, poor quality window choice $t \in [20, 30]$

Figure 7: Effective masses of $B^* - B$ ratio, obtained via fit to given window and the corresponding Bayesian weighting.

Acknowledgements

The numerical configuration generation (using the BQCD lattice QCD program [14])) and data analysis (using the Chroma software library [15]) was carried out on the DiRAC Blue Gene Q and Extreme Scaling (EPCC, Edinburgh, UK) and Data Intensive (Cambridge, UK) services, the GCS supercomputers JUQUEEN and JUWELS (NIC, Jülich, Germany) and resources provided by HLRN (The North-German Supercomputer Alliance), the NCI National Facility in Canberra, Australia (supported by the Australian Commonwealth Government) and the Phoenix HPC service (University of Adelaide). RH is supported by STFC through grant ST/P000630/1. PELR is supported in part by the STFC under contract ST/G00062X/1. GS is supported by DFG Grant No. SCHI 179/8-1. RDY and JMZ are supported by the Australian Research Council grant

DP190100297. SH is supported by the Bundesministerium für Bildung und Forschung (BMBF) 05H2021.

The authors at the University of Adelaide in Australia would like to acknowledge the Traditional Owners and Custodians of the lands that they live and work on. They pay their respects to the Kaurna people and to Indigenous Elders past, present and emerging. Sovereignty has never been ceded. It always was and always will be, Aboriginal land.

References

[1] Y. Amhis, S. Banerjee, E. Ben-Haim, F.U. Bernlochner et al., Heavy Flavour Averaging Group, *Averages of b-hadron, c-hadron, and τ-lepton properties as of 2018*, *The European Physical Journal C* **81** (2021) 226 [1909.12524].

[2] Y. Aoki, T. Blum, G. Colangelo, S. Collins et al., *FLAG review 2021*, 2111.09849.

[3] A. Bazavov, C. Bernard, N. Brown, C. DeTar et al., Fermilab Lattice and MILC Collaborations, *B- and D-meson leptonic decay constants from four-flavor lattice QCD*, *Phys. Rev. D* **98** (2018) 074512 [1810.00250].

[4] C. Hughes, C.T.H. Davies and C.J. Monahan, HPQCD Collaboration, *New methods for B meson decay constants and form factors from lattice NRQCD*, *Phys. Rev. D* **97** (2018) 054509 [1711.09981].

[5] P.A. Boyle, L.D. Debbio, N. Garron, A. Jüttner et al., *SU(3)-breaking ratios for $D_{(s)}$ and $B_{(s)}$ mesons*, 1812.08791.

[6] R. Balasubramamian and B. Blossier, *Decay constant of B_s and B_s^* mesons from $N_f = 2$ lattice QCD*, *The European Physical Journal C* **80** (2020) 412 [1912.09937].

[7] W. Bietenholz, V. Bornyakov, N. Cundy, M. Göckeler et al., QCDSF-UKQCD Collaboration, *Tuning the strange quark mass in lattice simulations*, *Physics Letters B* **690** (2010) 436 [1003.1114].

[8] W. Bietenholz, V. Bornyakov, M. Göckeler, R. Horsley et al., QCDSF-UKQCD Collaboration, *Flavor blindness and patterns of flavor symmetry breaking in lattice simulations of up, down, and strange quarks*, *Physical Review D* **84** (2011) 1 [1102.5300].

[9] A.X. El-Khadra, A.S. Kronfeld and P.B. Mackenzie, *Massive fermions in lattice gauge theory*, *Physical Review D* **55** (1997) 3933 [hep-lat/9604004].

[10] H.-W. Lin and N. Christ, *Nonperturbatively determined relativistic heavy quark action*, *Phys. Rev. D* **76** (2007) 074506 [hep-lat/0608005].

[11] Y. Aoki, N. Christ, J. Flynn, T. Izubuchi et al., RBC and UKQCD Collaborations, *Nonperturbative tuning of an improved relativistic heavy-quark action with application to bottom spectroscopy*, *Physical Review D* **86** (2012) 116003 [1206.2554].

[12] S. Beane, W. Detmold, R. Horsley, M. Illa et al., *Charged multihadron systems in lattice QCD+QED*, *Physical Review D* **103** (2021) [2003.12130].

[13] W.I. Jay and E.T. Neil, *Bayesian model averaging for analysis of lattice field theory results*, *Physical Review D* **103** (2021) [1003.1114].

[14] T.R. Haar, Y. Nakamura and H. Stüben, *An update on the BQCD Hybrid Monte Carlo program*, in *EPJ Web of Conferences*, vol. 175, p. 14011, EDP Sciences, 2018 [1711.03836].

[15] R.G. Edwards and B. Joó, *The Chroma software system for lattice QCD*, *Nuclear Physics B - Proceedings Supplements* **140** (2005) 832 [hep-lat/0409003].